Molecular Dynamics of Ionic Transport and Electrokinetic Effects in Realistic Silica Channels

Christian D. Lorenz*

Materials Research Group, Department of Mechanical Engineering, King's College London, London, UK WC2R 2LS

Paul S. Crozier

Sandia National Laboratories, Albuquerque New Mexico 87185

Joshua A. Anderson and Alex Travesset

Department of Physics and Astronomy and Ames Laboratory, Iowa State University, Ames, Iowa 50011

Received: December 6, 2007; Revised Manuscript Received: April 28, 2008

Silica is one of the most widely used inorganic materials in experiments and applications involving aqueous solutions of biomolecules, nanoparticles, etc. In this paper, we construct a detailed atomistic model of a silica interface that captures the essential experimentally known properties of a silica interface. We then perform all-atom molecular dynamics simulations of a silica nanochannel subjected to either an external pressure or an electric field and provide an atomistic description of ionic transport and both electro-osmotic flow and streaming currents for a solution of monovalent (0.4 M NaCl) as well as divalent (0.2 and 1.0 M $CaCl_2$) salts. Our results allow a detailed investigation of ζ-potentials, Stern layer conductance, charge inversion, ionic mobilities, as well as continuum theories and Onsager relations. We conclude with a discussion on the implications of our results for silica nanopore experiments and micro- and nanofluidic devices.

I. Introduction

Electrokinetic phenomena such as electro-osmotic flow (EOF), solvent flow induced by an external electric field, and streaming current (SC), the electric current resulting from an applied pressure gradient within a ionic solution, are classic effects in physical chemistry.[1] In recent years, electrokinetic effects have become an active area of research as they provide an elegant and precise tool to manipulate fluid motion at the nano- and microscales[2] and show potential for new sources of energy.[3,4] Furthermore, the development of synthetic nanopores as sensors for DNA, RNA, or proteins,[5] or of nanoporous functionalized silica thin films[6,7] for applications such as desalination membranes,[8] has prompted the need for an understanding of ionic transport and electrokinetic effects in confined geometries.

Models where both the solvent and ions are approximated as a continuum, such as the Poisson−Nernst−Planck (PNP) model,[1] provide the simplest and most widely used approach to electrokinetic phenomena and ionic transport. The PNP model, however, is strictly valid in the dilute limit only, where ionic activity coefficients are close to unity. Even in dilute systems, however, additional empirical corrections are often required. For example, experimental ζ-potential determinations can only be brought in agreement with theory by assuming the existence of Stern layer currents.[1,4,9,10] Further nuances arise for divalent ionic solutions, which, for example, show charge inversion (CI),[11] where an interface attracts charges in excess of its own nominal charge. The origins of CI are diverse,[12–14] and its description within continuum models still presents considerable challenges. In addition, effects related to the discrete nature of the solvent may play a dramatic role.[15]

Amorphous silica (SiO_2) has become one of the most widely used materials in wet technologies. Even synthetic nanopores made of Si_3N_4, commonly used in many DNA translocation experiments,[5,16] are usually treated on an oxygen plasma, in many cases leading to a pore covered with a thin SiO layer. Experimentally, silica interfaces have an intricate structure,[17] which has been mostly ignored in theoretical studies. The detailed modeling of the silica interface is critical for understanding electrokinetic and ion transport properties, even more so as the characteristic size shrinks to the nanometer scale, as in, for example, the physics of nanopores.[5]

In this paper we first present a model of a silica interface that closely approximates its known experimental properties. We further present all-atom molecular dynamics (MD) simulations of both EOF and SC on a silica nanochannel containing either monovalent or divalent ionic solutions. Besides providing a detailed description of ion transport and electrokinetic effects in silica channels, our study allows an atomistic study of problems that are still the subject of numerous controversies, such as the role of Stern layer currents or conduction "behind" the slip plane, ζ-potential determination or CI.

The electric current density J_{SC} resulting from a pressure gradient ∇P (the SC) and the water flow J_{EOF} arising from an electric field $E = -\nabla\varphi$ (the EOF), where φ is the externally applied electric potential, are given, in the linear regime, by eq 1,

$$J_{SC} = L_{21}(-\nabla P) J_{EOF} = \rho_w L_{12}(-\nabla\phi) \quad (1)$$

where ρ_w is the water density. The relation $L_{12} = L_{21}$[1] is a particular case of the Onsager reciprocal relations.[18] We point

* Corresponding author e-mail: chris.lorenz@kcl.ac.uk.

10.1021/jp711510k CCC: $40.75
Published on Web 06/14/2008

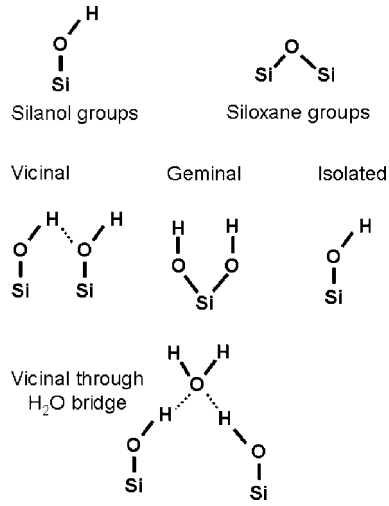

Figure 1. Types of groups that form a silica interface.

out, however, that to our knowledge, all explicit derivations of the symmetry relations implied by eq 1 have the PNP model as their starting point.[19]

Previous studies of electrokinetic phenomena by MD have been focused on all-atom simulations at the point of zero charge (pzc) of silica, either at zero ionic strength[20–22] or at 1 M NaCl using a specifically developed forcefield.[23] Other studies have focused on model surfaces in order to investigate effects related to surface roughness.[24] More coarse grained models[25] have been developed to provide a description of EOF at longer time scales.

II. Model of a Silica Interface

A. The Structure and Charge of a Silica Interface. The silica interface comprises two types of groups, silanol and siloxane groups, schematically represented in Figure 1. The siloxane groups are hydrophobic in character, whereas the silanol are hydrophilic.[26] The typical density of silanol groups is ~4.6 OH/nm^2.[17,26] Silanol groups are classified as isolated, vicinal, and geminal,[26] as depicted in Figure 1. Experimentally, according to the Zhuravlev model,[17] they are present in the following surface densities: 1.2, 2.80, and 0.60 OH/nm ^{2} for isolated, vicinal, and geminal, respectively. Recent experiments suggest that a significant fraction of vicinal groups consist, in fact, of two silanols not directly hydrogen bonded to each other, but through an intermediate water molecule (see Figure 1).[27–29]

The surface charge of a silica interface strongly depends on environmental variables such as pH, ionic strength, or temperature. Silica becomes electrically charged by releasing protons according to eq 2.

$$\mathrm{SiOH} + \mathrm{H_2O} \rightarrow \mathrm{SiO^-} + \mathrm{H_3O^+} \qquad (2)$$

In very acidic solutions (pH < 3), the silanol group may become positively charged by accepting protons. In basic solutions (pH > 9), silica significantly dissolves into silicate ions $HSiO_3^-$.[26] For these reasons, all subsequent analyses are restricted to the range 3 < pH < 9.

The simplest approach to predict the surface charge is to describe it by a triple model,[1] with a single pK_a and capacitance K_p. This was the approach followed by Bolt[30] and Schindler et al.[31] in the early literature. More recently, these results have been revisited by Behrens and Grier who proposed p$K_a \approx 7.5$ and $K_p \approx 2.9$ F/m ^{2}. However, these authors implicitly assume a density of silanol groups of 0.125 nm^2, which is a figure that is not supported by experiments.

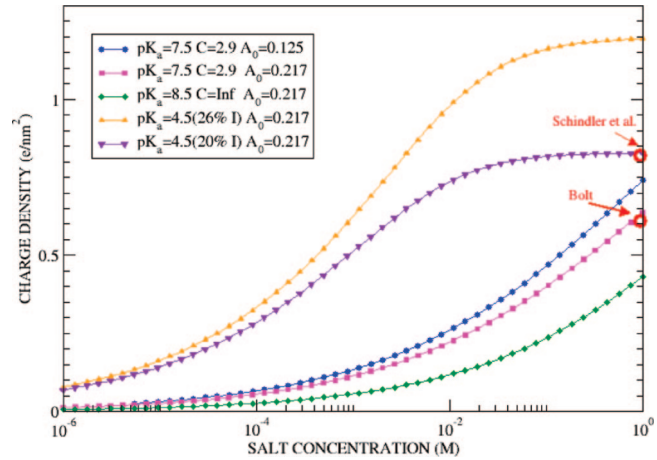

Figure 2. Predicted surface charge of silica as a function of monovalent ionic concentration at pH = 8 from the triple models,[1] with the parameters described in the text. The results of Bolt are quoted from ref 30 and Schindler et al. from ref 31. Units of capacitance (C) are F/m ^{2}, and that of area per charge (A_0) are nm^2.

A significantly more complex structure of the charging process of silica was revealed in the work of Ong et al.,[33] who from surface second harmonic generation experiments showed that 20% of silanol groups had a pK_a value of 4.5 and the remaining 80% had a pK_a value of 8.5. It was argued that the latter corresponds to vicinal silanols, where increased proton stability arises from hydrogen bonding to neighboring oxygens, whereas the former corresponds to isolated silanols. A sensible model for the charging process of silica is therefore provided by isolated silanols (between 20 and 26% of the silanol groups) having a pK_a = 4.5 and the remaining silanols (vicinal or geminal) with a pK_a = 8.5. The surface charge of silica as a function of salt concentration for different models at pH = 8 is shown in Figure 2. At large ionic strength, the differences are well-within experimental errors, but at low ionic strength, the triple models previously used in the literature, such as the one in ref predict a significantly larger deprotonation degree, which, most likely, explains the inability of previous triple models to describe SC flow with monovalent ions[34] in silica. Vicinal silanol groups form networks of hydrogen bonds, and the charging process becomes highly cooperative. In this regime, significantly more complex models have been developed.[29]

The charging process of silica in the presence of multivalent ions is also of interest for this paper. Experimental data on the surface charge of silica in the presence of divalent or trivalent ions is more scarce. From the early literature, we point out the work of Tadros and Lyklema,[35] who analyzed Ca^{2+} salts and concluded that, at high ionic strength, silica becomes significantly more charged for divalent ions than for monovalent ions. These results have been confirmed in ref 36, where a value of −1.21 e/nm^2 is quoted for 1.0 M $CaCl_2$ at pH = 8 and at room temperature. Streaming current measurements suggest a surface charge for silica on the order of −0.9 e/nm^2 at pH = 7.5,[11] consistent with the previous estimate. Quite interestingly, results for other divalent cations (Ba $^{2+}$ and Sr $^{2+}$) at pH = 8 are on the order of −0.9 e/nm^2[36] at pH = 8. The surface charge of silica in the presence of different trivalent ions has been studied with AFM tips[37] and yields a surface charge on the order of −2.2 e/nm^2, suggesting that all isolated and half of the vicinal silanol groups are deprotonated at salt concentrations larger than 0.1 mM. The charge of silica is, therefore, dependent not only on ionic strength but also on ionic valence.

B. Model of a Charged Silica Substrate. We first construct a silica interface with the distribution of vicinal, geminal,

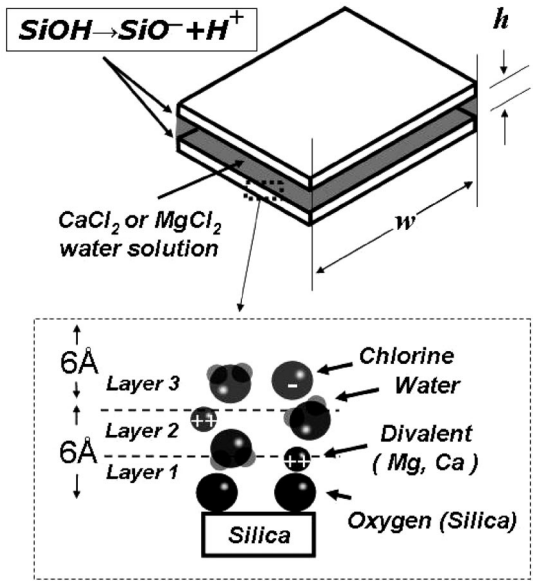

Figure 3. The silica channel consists of two interfaces separated a distance h. The layers next to the interface are defined as the inner Helmholtz plane (IHP), or layer 1, the outer Helmholtz plane (OHP), or layer 2, and the diffuse layer (DL).

and isolated silanol groups described by the Zhuravlev model. We define two silanols as vicinal if they can form a hydrogen bond, that is, if their oxygens are within 3 Å of one another, similar to the definition used in ref 38. A silanol is defined as isolated if it cannot form hydrogen bonds, which we define as having its nearest neighboring silanol more than 3 Å away. This description will suffice for the goals of this paper, but greater level of detail, such as vicinal silanol groups bridged by a water molecule (see Figure 1) or clusters of vicinal groups, can be incorporated following recent experimental results.[27–29]

The silica surface was generated from a bulk α-quartz silica crystalline solid, which was heated up to high temperatures (~2500 K) while using the BKS potential.[39] The system was then quenched to 300 K. Two free surfaces were generated along the z-dimension, and the substrate was annealed further at 300 K. The result of the quench is a certain number of under-coordinated silicons and oxygens. The resulting surfaces exhibit an overpopulation of isolated silanol groups, so the annealing was continued until the number of isolated silanol groups was reduced. By reducing the number of isolated silanol groups, we also reduce the overall density of silanol below the experimentally observed value.

To reach the experimental density of silanol groups, we randomly selected siloxane (Si−O) bonds that were within ~3 Å of either surface to be broken, similar to the method used in ref 38. We took care not to destroy any of the isolated silanols by ensuring that no bonds including the oxygens that are bonded to the silicons of the isolated silanol groups are removed. The resulting under-coordinated oxygens and silicons are terminated with −H and −OH groups, respectively. The resulting silica interface has a density of silanol groups of 4.6 OH/nm^2, such that the surface densities of the isolated, vicinal, and geminal silanol groups are 1.2, 2.8, and 0.6 OH/nm^2, respectively. Therefore, this results in a fully hydroxylated amorphous silica surface that closely resembles the Zhuravlev model of the silica interface.

The next step is to define the charges of the atoms and the different interaction potentials: the forcefield. In this paper we used a recent CHARMM forcefield that is specially designed for simulating charged amorphous silica in aqueous solutions.[38] (Note: we refer to this forcefield as the CHARMM water contact angle (CWCA) forcefield in order to differentiate it from the other CHARMM-based silica forcefields that have been generated for the α-quartz[40] and β-cristoballite[41] phases of silica.) The OPLS forcefield[42] used in ref[14] was not designed for simulating charged amorphous silica interfaces, so there are no predetermined rules for the charge assignment of a silanol group after it had been deprotonated. Therefore, we felt more comfortable using the CWCA forcefield[38] since it had been designed with applications similar to ours in mind.

The charges of the different silanol groups in the CWCA forcefield[38] are described by the following general rule,

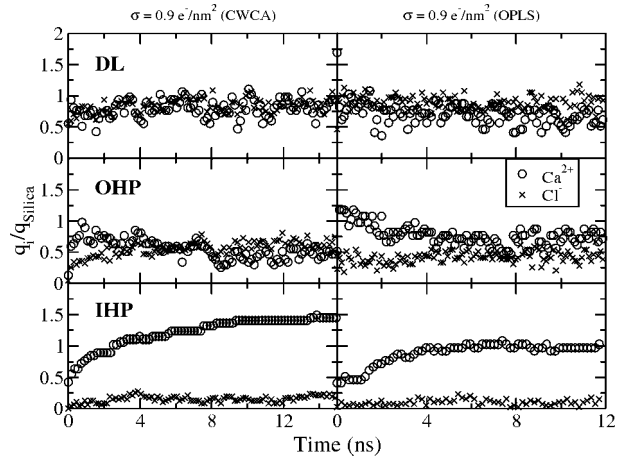

Figure 4. Evolution of the Ca^{2+} charge (○) and the Cl^- charge (×) relative to the interfacial charge as a function of time for the different layers (see Figure 3).

TABLE 1: Number of Bjerrum Pairs Per Cation for the Static Simulations of the 0.4 M NaCl, 0.2 M $CaCl_2$, and 1.0 M $CaCl_2$ systems[a]

region	0.4 M NaCl	0.2 M $CaCl_2$	1.0 M $CaCl_2$
IHP	0.05 (1)	0.26 (2)	0.56 (2)
OHP	0.09 (4)	0.50 (8)	0.89 (5)
DL	0.11 (5)	0.55 (8)	0.93 (5)
Bulk	0.15 (4)	0.61 (8)	0.94 (3)

[a] The numbers in the parentheses represent the error in the last digit of the stated value.

TABLE 2: Number of Nearest Neighbor Waters Per Ion for the 0.4 M NaCl, 0.2 M $CaCl_2$, and 1.0 M $CaCl_2$ Systems in the Various Layers near the Silica Interfaces for the Static Simulations[a]

System	Region	Cation	Anion
0.4 M NaCl	IHP	3.2 (1)	5.4 (4)
	OHP	5.5 (1)	7.0 (3)
	DL	5.5 (1)	7.2 (1)
	Bulk	5.4 (1)	7.2 (1)
0.2 M $CaCl_2$	IHP	5.0 (1)	5.5 (4)
	OHP	6.5 (4)	7.4 (1)
	DL	6.0 (5)	7.3 (1)
	Bulk	6.1 (2)	7.3 (1)
1.0 M $CaCl_2$	IHP	4.4 (1)	5.6 (3)
	OHP	4.5 (2)	7.2 (1)
	DL	4.4 (2)	7.0 (1)
	Bulk	4.4 (2)	7.0 (1)

[a] The numbers in parentheses represent the error in the last digit.

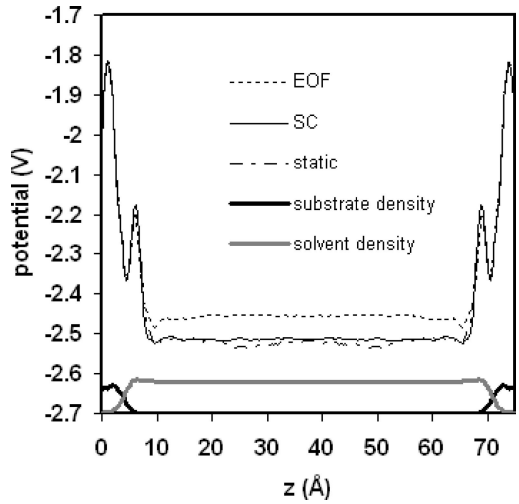

Figure 5. 1D electrostatic potential profile as a function of the z coordinate for the 1.0 M $CaCl_2$ static (dashed-dotted line), SC (thin solid line), and EOF (dashed line) cases. Solvent (thick gray line) and substrate (thick black line) atomic densities are shown in arbitrary units along the bottom for spatial reference. These densities, as well as the charge densities used to produce the potential profiles, have been symmetrized across the channel midplane

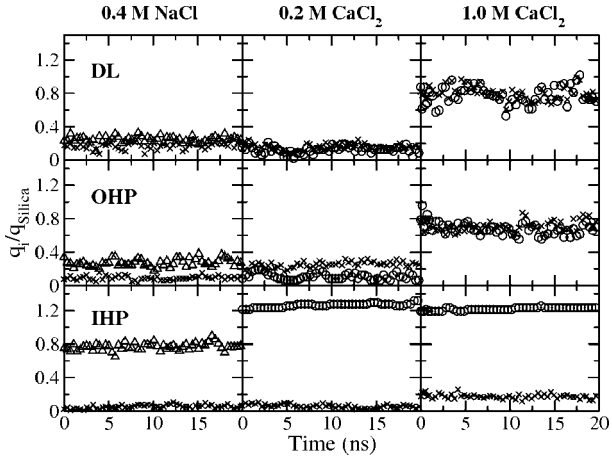

Figure 6. Evolution of the cation (Na^+ (Δ) or Ca^{2+} (○)) charge and the Cl^- charge (×) relative to the interfacial charge as a function of time for the different layers (defined in Figure 3) near the silica substrate for streaming current simulations.

$$q_{net} = q_{silanol} + q_{neighbor} \quad (3)$$

where q_{net} is the charge on a group of atoms containing a silanol (i.e., $q_{net} = 0$ for fully protonated silanol group(s), and $q_{net} = -1$ for deprotonated silanol group), $q_{silanol}$ is the sum of the charge of each atom within silanols, and $q_{neighbor}$ is the charge contribution from the oxygen atoms bonded to the silicon(s) in silanols. The detailed charge assignment schemes, which we have supplemented with additional rules to accommodate cases not described in the original CWCA forcefield, are described in detail, with concrete examples, in the Supporting Information.

The last step in the construction of the silica interface is the determination of which silanol groups are deprotonated. Obviously, the number of protons removed is dictated by experimental conditions. Following the discussion in Section II.A, protons are first randomly removed from isolated silanol groups, and only after all isolated silanol groups are deprotonated are the vicinal groups deprotonated. In this paper, we consider a system at pH ~7.5 and at room temperature, so only isolated silanol groups are actually deprotonated.

C. Description of Simulations. We consider a silica nanochannel as described in Figure 3. The dimensions of both silica substrates are 7.49948 × 6.94968 nm and are separated by a distance of $h = 7.5$ nm. We conducted a series of simulations with three ionic solutions: (1) 0.4 M NaCl, (2) 0.2 M $CaCl_2$, and (3) 1.0 M $CaCl_2$. From the discussion in Section II, the surface charge of silica at pH ~7.5 is about $\sigma = -0.9$ e/nm^2, consistent with experimental results[4] (note that the plot in Figure 2 is for pH = 8). As already pointed out, the surface charge has a dependence on ionic valence and strength, but the effects are relatively small for the cases discussed in our simulations, so we decided to treat the surface charge as constant, thus allowing an easier comparison of the different results.

Following our previous study,[14] we define three different layers; the first layer includes all partially dehydrated ions bound to the silica oxygens, the second layer consists of hydrated counterions immediate to the silica interface, and the third layer is defined as the intermediate region before bulk values are attained. In standard physical chemistry textbooks,[1] layers 1, 2, and 3 are referred to as the Inner Helmholtz plane (IHP), Outer Helmholtz plane (OHP), and the diffuse layer (DL), see Figure 3. Strictly speaking, both the IHP and OHP are layers, not planes, but we refer to them as planes so that our nomenclature remains consistent with that found in other literature. In this paper, these layers are defined by the distance (r_{ion}) between the center of the cation and the silica oxygen. Layer 1 (IHP) includes all counterions within $r_{ion} < 3$ Å, layer 2 (OHP) is those within 3 Å $< r_{ion} <$ 6 Å, and layer 3 (DL) is those within 6 Å $< r_{ion} <$ 12 Å, where the diameter of the water molecule is approximated as 3 Å.

The SC simulations presented in this paper were performed by considering a "gravity" field (or flow field)[43,44] instead of a pressure difference, as it is done in most experiments. Both a flow field and a pressure field lead to identical parabolic flows, but the former are easier to implement in MD. The small differences between a flow field or a pressure-induced field are irrelevant for the questions of interest in this paper.

The EOF simulations were performed by applying an external electric field $E = 0.5$ V/nm. The SC current simulations used a gravity field of 5×10^{-5} kcal/(Å gm), equivalent to a difference in pressure (ΔP) of 150 atm. Certainly, these large values may be of concern to experimentalists and some theorists, but the following arguments should provide some perspective. The electric field of a water molecule near a monovalent cation is $E \approx 20$ V/nm (40 times larger), and the isothermal compressibility of water, $\kappa_w \approx 5 \times 10^{-5}$ atm^{-1} implies that the pressure field induces a negligible volume compression $\delta V/V \approx 10^{-2}$. Although MD simulations with smaller electric and pressure fields would certainly be of interest, we contend that the present simulations allow for a very reasonable all-atom description of electrokinetic phenomena, a point that will become more apparent in the discussion section. Furthermore, the values of these external fields are in line with previous MD simulations.[23,24]

All the simulations reported in this paper were performed with the LAMMPS simulation package.[45] The parameters are from CHARMM,[38] and the TIP3P model for water[46] was employed. The silica substrate was not frozen, as has been done in previous simulations,[23] because this could induce an undesired temperature gradient (a thermophoretic effect). Each simulation was equilibrated for 10 ns, and runs with static configurations were conducted for 5 ns. All of the external field simulations

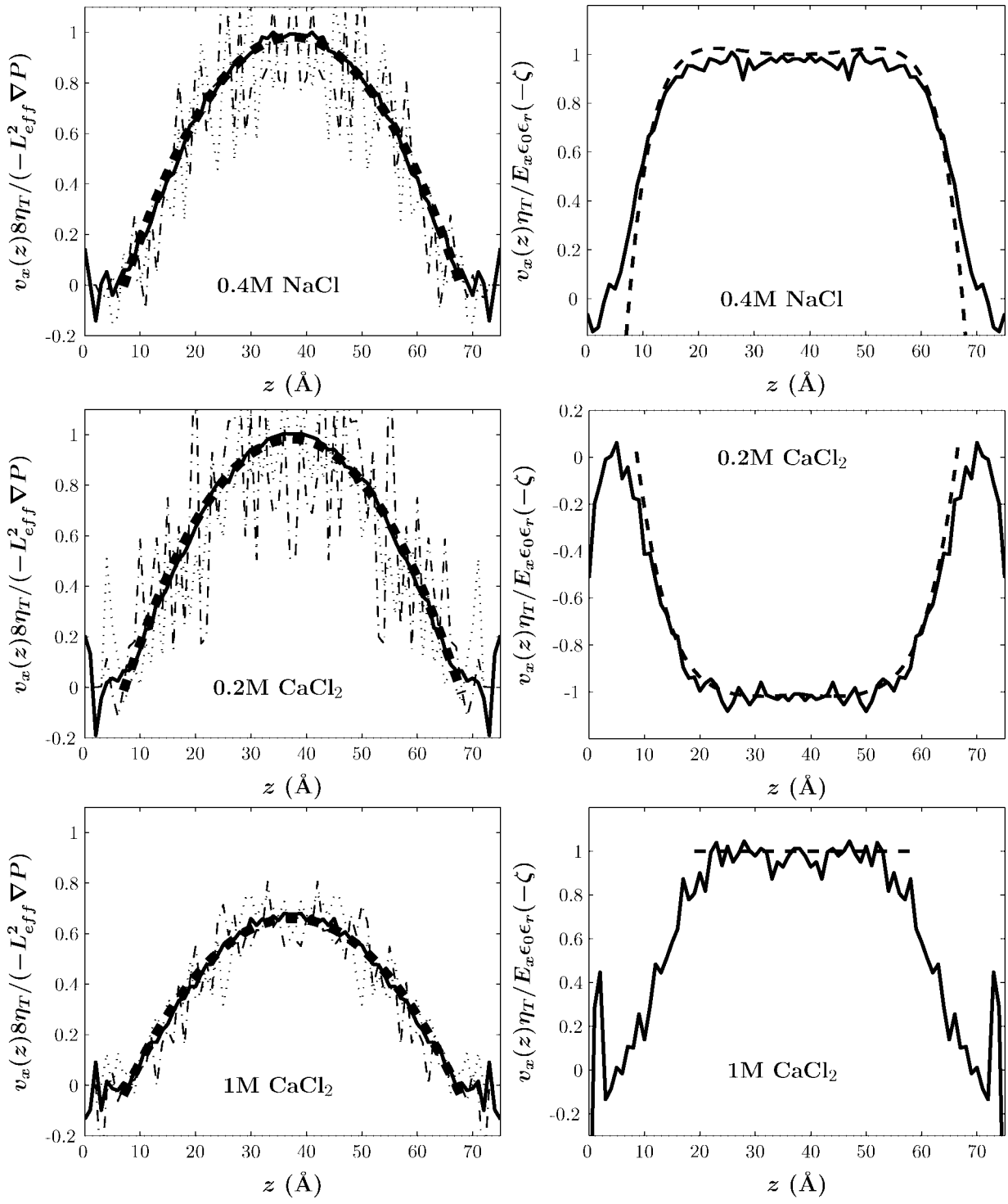

Figure 7. Velocity profiles (in normalized units) of the SC (left) and EOF (right) simulations. The solid lines are the water profiles, and the dashed lines are the theoretical formulas eqs 8 (SC) and 10 (EOF), with fitting parameters as discussed in the text. The dotted line and dashed-dotted line represent the cations and anions in the SC simulations. The 1.0 M $CaCl_2$ solution does not follow the continuum result eq 10, so only the flat region is indicated.

lasted for 20 ns and were conducted at 300 K under NVT conditions using the Nose−Hoover thermostat[47] and a 1 fs time step.

III. Results

A. Static Simulations. We report here the most salient results of the simulations in the absence of any applied field. These simulations can be directly compared with previous simulations conducted with the OPLS forcefield[42] and a different silica preparation method conducted by two of the authors.[14] A comparison of the OPLS results and the CWCA results for 1.0 M $CaCl_2$ in contact with silica substrates with two different surface charge densities ($\sigma = -0.9$ e/nm^2 and $\sigma = -2.0$ e/nm^2, the latter charge density can be achieved by tuning the pH) is included in the Supporting Information.

The population of the different layers for the 1.0 M $CaCl_2$ concentration are shown in Figure 4. The results show an excess of Ca^{2+} charge already in the IHP, thus giving raise to CI. The

TABLE 3: Net Molar, Mass, and Charge Fluxes of Water, Cation, and Anion in the 0.4 M NaCl, 0.2 M $CaCl_2$, and 1.0 M $CaCl_2$ Systems in the SC Simulations

system	species	molar flux (mol/nm^2 ns)	mass flux (amu/nm^2 ns)	charge flux (e$^-$/nm^2 ns)
0.4 M NaCl	H_2O	477 ± 34	8586	0.0
	Na^+	3.9 ± 3.2	90	3.9
	Cl^-	3.5 ± 1.6	124	−3.5
0.2 M $CaCl_2$	H_2O	471 ± 36	8478	0.0
	Ca^{2+}	0.92 ± 0.96	37	1.8
	Cl^-	2.2 ± 0.87	78	−2.2
1.0 M $CaCl_2$	H_2O	300 ± 33	5400	0.0
	Ca^{2+}	4.9 ± 2.8	196	9.8
	Cl^-	10.8 ± 4.0	383	−10.8

TABLE 4: Net Molar Fluxes (mol/nm^2 ns) of Water, Cation, and Anion in Each Layer of the 0.4 M NaCl, 0.2 M $CaCl_2$, and 1.0 M $CaCl_2$ Systems in the SC Simulations

system	species	IHP	OHP	DL	bulk
0.4 M NaCl	H_2O	1.50	9.87	52.40	404.11
	Na^+	0.01	0.10	0.53	3.29
	Cl^-	0.01	0.05	0.35	3.23
0.2 M $CaCl_2$	H_2O	0.97	7.87	50.24	406.53
	Ca^{2+}	0.00	−0.01	0.10	0.92
	Cl^-	−0.01	0.04	0.24	2.00
1.0 M $CaCl_2$	H_2O	0.70	3.96	28.66	260.80
	Ca^{2+}	0.01	0.03	0.40	4.51
	Cl^-	0.01	0.06	0.83	8.98

residence times of Ca^{2+} are significant (~5.0 ns), leading to long equilibration times. For comparison, the results with the OPLS forcefield[14] are also shown. Although both forcefields give similar amounts of CI and pair distribution functions (results not shown), the population of the different layers is somewhat different. When using the OPLS forcefield, there is no CI at the IHP, it arises entirely from the OHP. Consistently, the residence times in the IHP are about 2 ns, much shorter than the residence times observed in the present simulations. A more surprising result is that the CWCA forcefield shows CI at 0.2 M $CaCl_2$ whereas previous results with the OPLS forcefield[14] indicated that CI disappears below 0.4 M, which is in better agreement with experimental results.[11] This seems to point out a deficiency in the CWCA forcefield, a point that will be discussed in greater detail in the following paragraphs.

Formation of Bjerrum pairs and ionic hydration numbers are important effects readily accessible by MD. To identify both Bjerrum pairs and hydration numbers, we used a simple distance criterion, where an atom A and an atom B are nearest neighbors (NN) if they are within a distance $r_{AB} \equiv r_A + r_B + r_{cut}$, where r_J is the crystallographic radius of atom J and $r_{cut} = 0.5$ Å is a cutoff that allows atoms to be considered a Bjerrum pair even if not in direct contact. Similar results are obtained by defining the Bjerrum pairing from the first minimum in the pair distribution functions. Results are summarized in Tables 1 and 2.

The Bjerrum pairing results are summarized in Table 1. The Bjerrum pairing at the IHP is greatly reduced by the competition from the interface, as ions bound to the silanol oxygens have less accessible area to bind other ions. In the subsequent layers, Bjerrum pairing is approximately the same as in bulk. Clearly, divalent ions show larger amounts of Bjerrum pairing than monovalent ions. At 1.0 M $CaCl_2$, there are almost no free (unpaired) Ca^{2+} ions. This trend of increasing number of paired Ca^{2+} ions with increased ionic concentration is due to the fact that at higher ionic concentration it is more likely for the Ca^{2+} and Cl^- ions to be near one another and therefore be paired.

Table 2 summarizes the hydration numbers for the cations and anions in the various layers near the silica interface for the three different systems. In most cases, there is a noticeable surface effect causing the hydration number for both the cation and anion to be smaller in the IHP as compared to that found in the other three layers. Rather interestingly, the hydration number of the Ca^{2+} ions in the 1.0 M $CaCl_2$ system is significantly smaller than for the 0.2 M $CaCl_2$ system, which reflects the larger degree of Bjerrum pairing.

The electrostatic potential profiles across the channel were computed using an integrated form of the Poisson equation and appropriate boundary conditions. We start with the Poisson equation in the form shown in eq 4,

$$\frac{d^2\varphi}{dz^2} = -\frac{1}{\varepsilon_o}\sum_i q_i\rho_i(z) \tag{4}$$

where ϕ is the electric potential, ε_o is the vacuum permittivity constant, the summation over the index i refers to the various atom types, q_i is the charge on atoms of type i, ρ_i is the density of atoms of type i, and z is the distance in the direction perpendicular to the surface of the substrate. After integrating twice and applying boundary conditions such that the potential and its gradient are zero outside of the silica layers, we get the one-dimensional (1D) integrated form of the Poisson equation as eq 5,

$$\varphi(z) = -\frac{1}{\varepsilon_o}\sum_i q_i\int_0^z (z-u)\rho_i(u)\,du \tag{5}$$

where the integral is performed numerically using binned charge distributions from snapshots of the simulated systems. The results for the 1.0 M $CaCl_2$ cases (see Figure 5) show a relatively flat plateau corresponding to the aqueous ionic solution and a jump of the potential as the silica interface is crossed. The interface region exhibits a detailed structure that will be discussed below.

Also of interest is the displacement vector, defined by eq 6,

$$\frac{dD(z)}{dz} = \sum_i q_i^f\rho_i(z) \tag{6}$$

where the free charges q_i^f are all system charges except the water. The "continuum" electric field within the solution is obtained from eq 7,

$$E_c(z) = D(z)/(\varepsilon_0\varepsilon_r) \tag{7}$$

where ε_r is the water dielectric constant ($\varepsilon_r \approx 70$ for the TIP3P model). As the silica interface is approached, ε_r decreases from its value in solution, but the discussion of this effect is not necessary for the goals of this paper.

B. Streaming Current Simulations. The velocity profile is expected to follow the Poiseuille formula, with its characteristic parabolic profile (eq 8),

$$v_x^{SC}(z) = -\frac{\nabla P}{2\eta}(z-L_s)(h-L_s-z) \tag{8}$$

where L_s defines the position of the shear plane (the plane where the fluid velocity vanishes). The shear viscosity (η) of the TIP3P model is given by $\eta_T = 0.31$ cp, about 2.9 times smaller than the one of water at the same temperature.[48] We recall that most theoretical descriptions assume that the position of the shear plane coincides with the boundary between the OHP and the DL.[1,14]

We first analyze the populations of the different layers (defined in eq 3). The results show a remarkable stability of

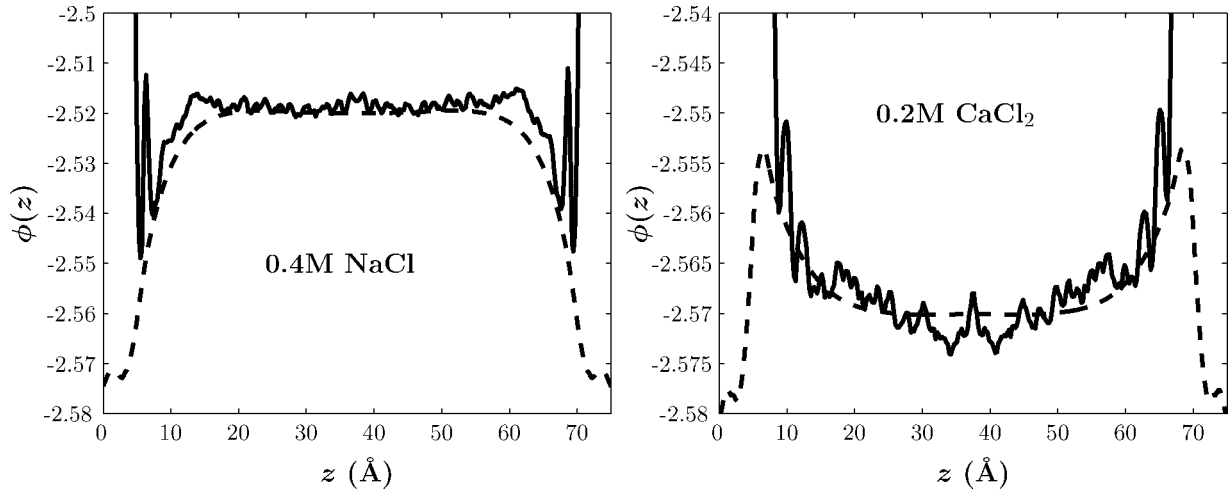

Figure 8. Comparison between the electric potential for the EOF computed with explicit water (solid curve) and the result with a continuum dielectric constant (dashed curve).

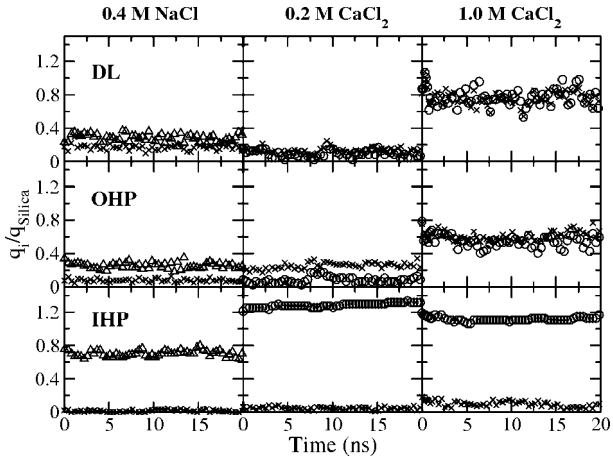

Figure 9. Evolution of the cation (Na^+ (Δ) or Ca^{2+} (○)) charge and the Cl^- charge (×) relative to the interfacial charge as a function of time. The different layers are defined in Figure 3.

the populations within the different layers (see Figure 6), thus providing clear evidence that the system has reached steady state. Compared with the static case, the actual differences are not very significant.

The velocity profiles obtained from the SC simulations are shown in Figure 7 and exhibit the expected parabolic profile. If, following previous considerations, the position of the shear plane is fixed at the boundary between the OHP and the DL ($L_s \approx 6$ Å), then the Poiseuille formula (eq 8) describes the flows for the 0.4 M NaCl and 0.2 M $CaCl_2$ systems without any need for fitting parameters. Although the velocity flows for the 1.0 M $CaCl_2$ system still follow the expected parabolic profile, in order to describe the flow with eq 8, the viscosity of the system is left as a free parameter $\eta_{T,\,1.0M}$, yielding eq 9.

$$\eta_{T,1.0M}/\eta_T \approx 1.7 \tag{9}$$

That is, at 1.0 M $CaCl_2$ the aqueous solution shows a large electroviscous effect.

Table 3 summarizes the main quantitative results of the simulations, namely, the net molar, mass, and charge fluxes (normalized by the total channel width) for water, cations, and anions. Table 4 summarizes the molar flux of the various species in each layer. The molar flux of each species was calculated by counting the number of times each molecule of a specific type spanned the length of the nanochannel in the x-dimension and then dividing that value by the total time over which the value was obtained and the cross-sectional area of the nanochannel ($l_y \times l_z$). In the case of the values in Table 4, these flux values were binned based on the location of each molecule in the z-dimension. The SC was obtained by subtracting the net charge flux of cations from the anions.

C. Electro-osmotic Flow Simulations. The velocity profiles of the water under EOF conditions are expected to follow the Smoluchowsky formula (eq 10),

$$v_x(z) = -\frac{\varepsilon_0 \varepsilon_r}{\eta}(\eta - \varphi(z) + \varphi(h/2))E_x \tag{10}$$

where $\phi(z)$ is the electric potential and $\phi(h/2)$ is the value of the potential at the midplane of the channel (in most textbooks the potential is already defined such that $\phi(h/2) \equiv 0$). The Debye length is $\lambda_D > 10$ Å for all ionic concentrations discussed in this paper, so the potential reaches its midplane value at about 10 Å. The water velocity profile is therefore expected to exhibit a plug-type shape, where for $z \gg \lambda_D$ the water flow moves at a constant velocity $v_x = -\varepsilon_0 \varepsilon_r E_x/\eta\zeta$. The quantity ζ is the difference in potential between the midplane (the bulk) and the interface and is known as the ζ-potential.[1]

The simulation results for the population of the different layers, shown in Figure 9, again provide clear evidence that the system has reached steady-state. Similarly as with SC, the relative populations were not greatly affected by the presence of external perturbations.

The water velocity profile, shown in Figure 7, exhibits the expected plug-type flow. The electrostatic potential profile including the water explicitly is somewhat noisy, but the implicit electrostatic potential profile, defined in eq 7 is smooth and agrees with the explicit water result in the relevant region, as shown in Figure 8. We therefore use the latter potential in the Schmoluchowsky formula, which allows us to determine the ζ-potential. A detailed discussion of the ζ-potential is further elaborated in the following section.

The ionic velocity profiles, normalized as in Figure 7, are shown in Figure 10. The results for 0.4 M NaCl and 0.2 M $CaCl_2$ show the expected behavior, where cations and anions move along in opposite directions. The 1.0 M $CaCl_2$ simulations, however, shows both anions and cations moving in the same direction. It should be noted, however, that the anions move slightly slower than the water, so relative to the water, the anions are still moving in an opposite direction with respect to the

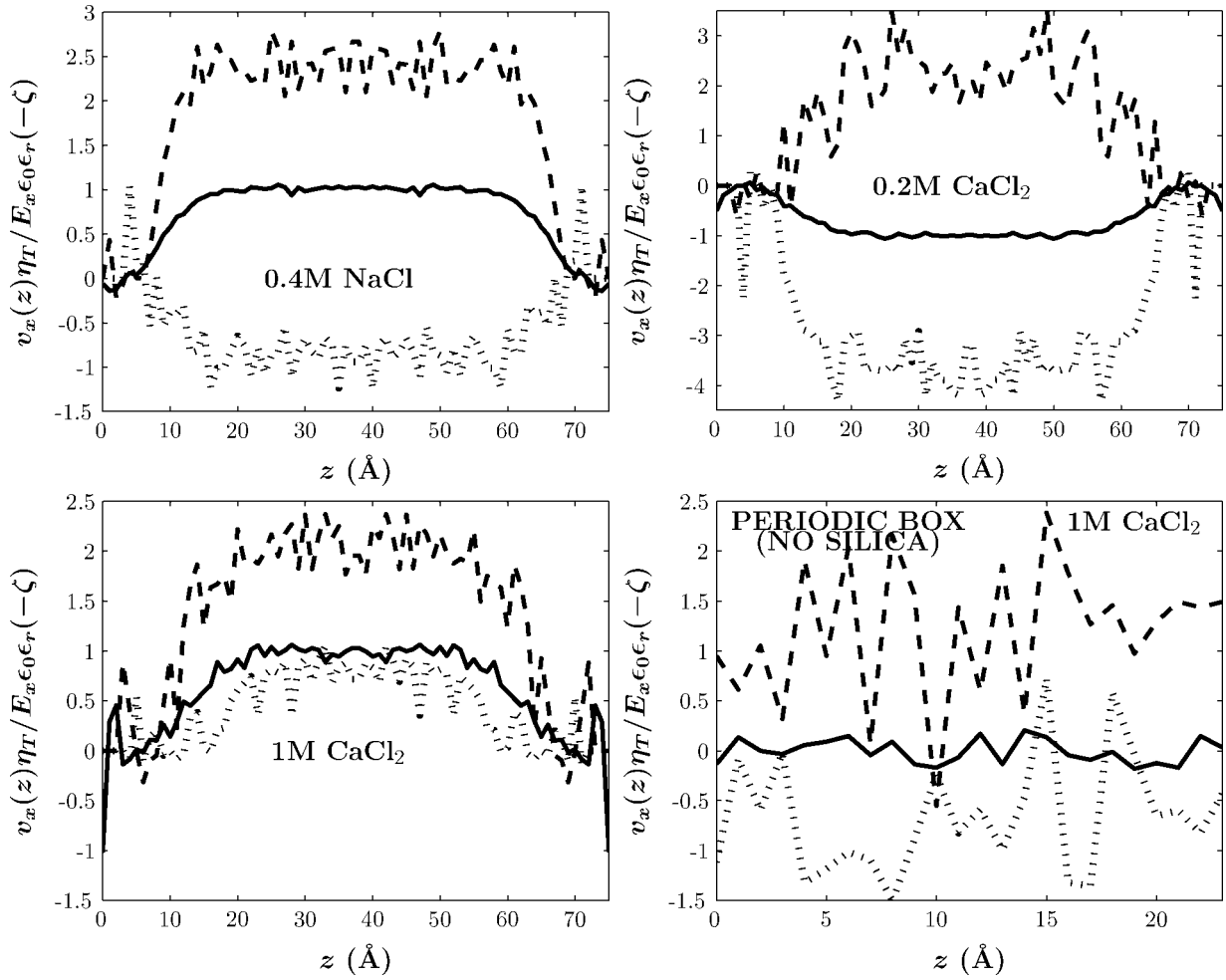

Figure 10. Velocity profiles for the water (solid line), cations (dashed line), and anions (hashed line). The bottom right figure represents data collected over 5 ns from a simulation of a periodic box containing 1.0 M $CaCl_2$, without any silica interface. The data for the bulk simulation was normalized in the same fashion as the data from the nanochannel data (left bottom).

TABLE 5: Net Molar, Mass, and Charge Fluxes of Water, Cation, and Anion in the 0.4 M NaCl, 0.2 M $CaCl_2$, and 1.0 M $CaCl_2$ Systems in the EOF Simulations

system	species	molar flux (mol/nm^2 ns)	mass flux (amu/nm^2 ns)	charge flux (e$^-$/nm^2 ns)
0.4 M NaCl	H_2O	484.7 ± 127.6	8725	0.0
	Na^+	12.2 ± 4.9	281	12.2
	Cl^-	−3.5 ± 3.2	124	3.5
0.2 M $CaCl_2$	H_2O	−235 ± 128	−4230	0.0
	Ca^{2+}	1.22 ± 1.39	49	2.44
	Cl^-	−4.49 ± 1.96	−160	4.49
1.0 M $CaCl_2$	H_2O	172 ± 85	3096	0.0
	Ca^{2+}	6.84 ± 3.64	274	13.7
	Cl^-	4.21 ± 5.14	150	−4.21

cations. The direction of the anions is therefore the result of hydrodynamic drag dominating over electric migration. More surprising, however, is that the EOF is in the opposite direction as it would be expected from a negatively charged DL (see Figure 9). To rule out the possibility of simulation artifacts, we carried out a control simulation consisting of an equilibrated periodic box of water containing 1.0 M $CaCl_2$ (without any interface) and subjected it to the same external conditions as if the silica were present. The results are shown in Figure 10 (bottom right) and show the expected results: anions and cations moving in opposite directions and no induced EOF. The observed anomalous EOF at 1.0 M $CaCl_2$ is, therefore, a real physical effect.

TABLE 6: Net Molar Fluxes (mol/nm^2 ns) of Water, Cation, and Anion in Each Layer of the 0.4 M NaCl, 0.2 M $CaCl_2$, and 1.0 M $CaCl_2$ Systems in the EOF Simulations

System	Species	IHP	OHP	DL	Bulk
0.4 M NaCl	H_2O	3.84	24.88	89.28	362.65
	Na^+	0.12	1.00	2.83	8.08
	Cl^-	−0.01	−0.10	−0.59	−2.89
0.2 M $CaCl_2$	H_2O	−1.61	−5.62	−35.34	−187.67
	Ca^{2+}	0.00	0.01	0.09	1.09
	Cl^-	−0.01	−0.17	−0.95	−3.79
1.0 M $CaCl_2$	H_2O	0.28	5.34	23.39	138.99
	Ca^{2+}	0.00	0.10	0.90	5.52
	Cl^-	−0.01	−0.04	0.18	3.47

TABLE 7: Values of the ζ-Potential Calculated from SC and EOF Simulations

system	ζ (EOF) (mV)	ζ (SC) (mV)
0.4 M NaCl	−21	−21
0.2 M $CaCl_2$	11	17
1.0 M $CaCl_2$	−19	46

Table 5 summarizes the main quantitative results of the EOF simulations, namely, the net molar, mass, and charge fluxes (normalized by the total channel width) for water, cations, and anions. The net molar quantities for the various species in the various layers near the silica interface are also shown in Table 6 and were computed by the same methods as described in Section III.B.

IV. Discussion

A. Ionic Mobilities. Ionic mobilities of species a are defined by eq 11,

$$u^a = \frac{v_x^a}{E_x} \quad (\text{units of } \mathrm{cm^2 V^{-1} s^{-1}}) \tag{11}$$

where E_x is the external field and v_x^a is the bulk ionic velocity. In our system, however, once the electric field is applied, the solvent is not at rest because of the EOF. The mobilities are defined in the reference frame where the solvent is at rest, hence eq 12 is obtained.

$$u^a = \frac{v_x^a - v_x^{\mathrm{EOF}}}{E_x} \tag{12}$$

From the results in Section III.C one obtains that $v_x^{\mathrm{EOF}} \approx 20$ m/s, $v_x^{\mathrm{Na}} \approx 50$ m/s, and $v_x^{Cl} \approx -20$ m/s. Application of eq 12, gives $u^{\mathrm{Na}} \approx 6 \times 10^{-4}$ cm^2/(Vs) and $u^{\mathrm{Cl}} \approx 8 \times 10^{-4}$ cm^2/(Vs) for the 0.4 M NaCl system. A similar calculation for the 0.2 M $CaCl_2$ system yields similar values for u^{Cl} and $u^{\mathrm{Ca}} \approx 4 \times 10^{-4}$ cm^2/(Vs). At the ionic concentrations considered in our study, electrophoretic and relaxation forces should provide significant contributions. Our results for mobilities compare surprisingly well with precise calculations in the dilute limit.[49] These results provide reassurance that the large values for the external fields do provide a reasonable description of ionic transport and electrokinetic effects.

The mobilities of EOF at 1.0 M $CaCl_2$ are much smaller than in the other two cases discussed. This is particularly true for the Cl^- ions, whose mobility is 1 order of magnitude smaller. This reduction in the mobility is related to the strong Bjerrum pairing observed (see Table 1), which is suggestive of a dominance of relaxation and electrophoretic forces and is also reflected in the large electroviscous effect.

B. The Onsager Relations. The Onsager relations have been introduced in eq 1. The electric current density J_{SC} from the SC simulations and the water flow J_{EOF} from the EOF simulations are computed from Tables 3 and 5, respectively. The external fields are also known to be $E_x = 0.05$ V/Å and $\nabla P = 2.1 \times 10^{15}$ Pa/m. Therefore, for the 0.4 M NaCl system we obtain eq 13.

$$\frac{L_{21}}{L_{12}} = \frac{J_{\mathrm{SC}} E_x}{J_{\mathrm{EOF}} \nabla P} \approx 1.05 \pm 0.55 \tag{13}$$

The relatively large error bars arise from the fact that the relevant currents are obtained by subtracting similar quantities. To our knowledge, all explicit derivations of Onsager relations[19] have the PNP model at its starting point, so our results clearly suggest that a similar derivation could be extended to more concentrated regimes, where ionic correlations are important. At 0.2 M $CaCl_2$ the same calculation gives eq 14.

$$\frac{L_{21}}{L_{12}} = \frac{J_{\mathrm{SC}} E_x}{J_{\mathrm{EOF}} \nabla P} \approx 1.8 \pm 0.6 \tag{14}$$

Some deviations from unity are observed but are not very significant.

The 1.0 M $CaCl_2$ system does present a clear violation of the Onsager relations as expressed by eq 1, as both the SC and the EOF point in different directions. The anomaly, as it has been emphasized, lies in the direction of the EOF, which behaves as if the DL were positively charged. Furthermore, the presence of the silica interface is critical for this phenomenon, as is clear from Figure 10. Here we recall that a number of effects occur at 1.0 M $CaCl_2$; almost all Ca^{2+} ions are paired (see Table 1), and approximately half of the water molecules are "dead water" (water molecules that are in the hydration sheath or directly correlated to it). Our interpretation of the anomalous EOF is that the bulk Ca^{2+} ions, which have a very compact hydration sheath, are more effective in dragging water molecules than the corresponding anions, and the no-slip boundary condition set up by the interface sets the bulk water molecules in motion. A more detailed analysis of this effect will be discussed elsewhere.

C. The ζ-Potential. The ζ-potential within SC experiments can be obtained using the approximation that the channel length is much larger than the Debye length and integrating eq 8,[1]

$$\zeta = \frac{I_{\mathrm{str}} \eta}{\varepsilon_0 \varepsilon_r A \nabla P} \tag{15}$$

where I_{str} is calculated from Table 3, A is the effective channel area, and the values of the other parameters are known. The ζ-potential is defined as the potential drop from the shear plane to the midplane. The position of the shear plane must be identified as the boundary between the DL and the OHP planes, and indeed the calculated value of the ζ-potential from eq 15 agrees with the value of the potential difference computed in this way. The calculated values of the ζ-potential are shown in Table 7.

The ζ-potential is also obtained from the plug-flow velocity in the EOF, as already discussed in Section III.C. However, it should be noted that the validity of the obtained ζ-potential hinges on the validity of the theoretical expression eq 10, which fails for the 1.0 M $CaCl_2$ solution as discussed. Therefore, the EOF value quoted in Table 7 for the 1.0 M $CaCl_2$ does not have the physical meaning of the difference in electrostatic potential between the bulk and the shear plane.

One important point to notice, however, is that the position of the shear plane in the EOF ζ-potential is not determined as precisely as in SC flows. Also, as is clear from Figure 8, the electric potential changes very rapidly as it approaches the silica interface, so the determination of the ζ-potential is not possible without a very precise definition of where the shear plane is.

D. Ionic Conduction Behind the Slip Plane. The breakdown of the molar fluxes of the different ionic species within each layer (defined in Figure 3), presented in Table 5, shows a significant current within both the IHP and the OHP, which is known as "conduction behind the slip plane".[9,10] This current is negligible for divalent ionic solutions. This is expected, given the long residence times and compact hydration sheath of Ca^{2+} at silica interfaces. For NaCl however, there is a significant ionic conduction behind the slip plane. Clearly, its presence does not yield a significant contribution to the ζ-potential.

V. Conclusions

We have conducted MD simulations of electrokinetic effects, both SC and EOF, and of ionic transport in silica nanochannels using all-atom molecular dynamics. We emphasized the importance of a precise description of the complex properties of silica interfaces and provided an explicit algorithm to accurately model these properties. Our results show that MD is able to provide a description of electrokinetic effects with atomic resolution. As it is clear from the obtained parabolic and plug-type flow for SC and EOF, respectively, as well as the calculated mobilities, electric potentials, etc., the large values of external electric and pressure fields at which our simulations were run do not limit the fundamental implications of our results for the significantly smaller external fields used in most experiments.

Our study of monovalent solutions, performed at 0.4 M NaCl concentration, show a textbook description of both EOF and SC. Our computed flow in SC simulations are described by the Poiseuille parabolic formula without any fitting parameters if the shear plane is made to coincide with the beginning of the DL (see Figure 3), as it has been assumed in virtually all previous theoretical descriptions.[1] The flows in EOF show the expected plug-type shape and are well-described by the continuum Schmoluchowsky formula eq 10. Our results show that electrokinetic effects can be computed if the charge distribution ρ^f (or the potential) is known in the static case. The charge distribution ρ^f (or the potential) in the static case can be easily computed from simulations, or in the dilute limit it can be approximated by a Boltzmann description, which leads to a self-consistent set of equations, the PNP model. For monovalent solutions, despite the important role of ionic correlations, the PNP model can provide a qualitative description, although for more-realistic quantitative analysis the exact potential profile must be determined.

Divalent ionic solutions show a more complex behavior. Both simulations performed at 0.2 M $CaCl_2$ and 1.0 M $CaCl_2$ show charge inversion. The 0.2 M $CaCl_2$ flow in SC simulations follows the Poiseuille flow without fitting parameters. The significant amount of Bjerrum pairing, however, has an important effect on the EOF, which is likely related to the slight deviations observed in the Onsager relations. The 1.0 M $CaCl_2$ solutions show very interesting features. The SC flow follows the characteristic Poiseuille profile, but the viscosity is increased by almost a factor of 2, indicative of a considerable electroviscous effect. The understanding of electroviscous effects at high ionic strength and high valence is still somewhat primitive,[50] so direct comparison with theories is not yet possible. At high ionic strength and high valence, we have shown that the EOF is anomalous and briefly discussed its relation to Bjerrum pairing as well as the presence of large amounts of dead water.

Our studies made use of the CHARMM forcefield introduced by Cruz-Chu et al.,[38] which we have referred to as the CWCA forcefield. The CWCA forcefield in a 0.2 M $CaCl_2$ solution exhibits CI, which is in disagreement with experimental results[4] that report that CI should disappear below 0.4 M $CaCl_2$. The CWCA forcefield was derived from the wetting properties of silica, and it therefore significantly depends on the model used for the silica interface. It remains as a future task to investigate how the CWCA forcefield would be modified by considering the silica model interface proposed in this paper. Also relevant for an accurate model is the role of the low viscosity of the TIP3P water model. Since all transport properties depend on shear viscosity, water models that accurately model dynamic properties are of utmost relevance. MD simulations using, for example, the SPC/E model,[51] which has a viscosity closer to the one of real water ($\eta_{SPC/E} = 0.73\eta_W$),[52] should be able to unambiguously establish the possible dependence of the presented results on the actual value of the viscosity.

We discuss the implications of our results for fluidic devices and nanopore experiments. As a general rule, if one knows the pH and/or ionic concentration of the system of interest, then an accurate model of the silica interface can be produced using the general methods outlined in this article. Then, both ionic transport and electrokinetic effects can be modeled very accurately by a multiscale approach, where electric potentials and charge distributions are determined from an atomistic simulation in the static case and then using the continuum results (Poiseuille flow, Schmoluchosky equation, etc.) to model transport properties. Our detailed model of the silica interface is pertinent to nanopore experiments. Experimentally, the fabrication of accurate and reliable synthetic nanopores is challenging,[5] and understanding the magnitude of the ionic currents passing through the nanopore is even more difficult. The results of this paper can be used to model the detailed structure of a silica nanopore with a realistic description of silanol and siloxane groups, and thus provide an unambiguous understanding of how interfacial effects control transport properties. We hope to report more in the near future.

Acknowledgment. We thank J. Faraudo and J. Lyklema, as each provided a careful reading of the manuscript and many insightful comments, and also E. Cruz-Chu and D. Stein for discussions regarding various aspects of this study. C. D. L. thanks E. B. Webb III for past discussions of the surface chemistry of silica. The work of A. T. and J. A. A. has been supported by NSF grant DMR-0426597 and partially supported by DOE through the Ames laboratory under contract No. DE-AC02-07CH11358. P. S. C. has been supported by Sandia National Laboratories LDRD project 90493/08.05. Sandia is a multiprogram laboratory operated by Sandia Corporation, a Lockheed Martin Company, for the United States Department of Energy's National Nuclear Security Administration under contract DE-AC04-94AL85000.

Supporting Information Available: A detailed description of the forcefield parameters used for the CWCA forcefield. A detailed description of the charge assignment methodology for the protonated and deprotonated isolated, vicinal, and geminal silanol groups. A thorough comparison of the CWCA and OPLS forcefields as well as a comparison of the effect of the surface charge density on the charge inversion properties of the 1.0 M $CaCl_2$ system. This material is available free of charge via the Internet at http://pubs.acs.org.

References and Notes

(1) Lyklema, J. *Fundamentals of Interface and Colloid Science*; Academic Press: San Diego, 1995.
(2) Stone, H. A.; Stroock, A. D.; Ajdari, A. *Annu. Rev. Fluid Mech.* **2004**, *36*, 381.
(3) Yang, J.; Lu, F.; Kostiuk, L. W.; Kwok, D. Y. *J. Micromech. Microeng.* **2003**, *13*, 963.
(4) van der Heyden, F. H. J.; Bonthuis, D. J.; Stein, D.; Meyer, C.; Dekker, D. *Nano Lett.* **2006**, *6*, 2232.
(5) Dekker, C. *Nat. Nanotech.* **2007**, *2*, 209.
(6) Doshi, D. A.; Huesing, N. K.; Lu, M.; Fan, H.; Lu, Y.; Simmons-Potter, K.; Potter, B. G.; Hurd, A. J.; Brinker, C. J. *Science* **2000**, *290*, 107.
(7) Liu, N. G.; Assink, N. A.; Brinker, C. J. *Chem. Commun. (Cambridge)* **2003**, *3*, 370.
(8) Leung, K.; Rempe, S. B.; Lorenz, C. D. *Phys. Rev. Lett.* **2006**, *96*, 095504.
(9) Hidalgo-Álvarez, R.; Martín, A.; Fernández, A.; Bastos, D.; Martínez, F.; de las Nieves, F. J. *Adv. Colloidal Interface Sci.* **1996**, *67*, 1.
(10) Hunter, R. J. *Adv. Colloidal Interface Sci.* **2003**, *100*, 153.
(11) van der Heyden, F. H. J.; Stein, D.; Besteman, K.; Lemay, S. G.; Dekker, C. *Phys. Rev. Lett.* **2006**, *96*, 224502.
(12) Lyklema, J. *Coll. and Surf. A* **2003**, *291*, 3.
(13) Faraudo, J.; Travesset, A. *J. Chem. Phys. C* **2007**, *111*, 987.
(14) Lorenz, C. D.; Travesset, A. *Phys. Rev. E* **2007**, *75*, 061202.
(15) Faraudo, J.; Bresme, F. *Phys. Rev. Lett.* **2004**, *92*, 236102.
(16) Heng, J. B.; Aksimentiev, A.; Ho, C.; Marks, P.; Grinkova, Y. V.; Sligar, S.; Schulten, K.; Timp, G. *Nano Lett.* **2005**, *5*, 1883.
(17) Zhuravlev, L. T. *Colloids Surf. A.* **2000**, *173*, 1.
(18) Groot, S. R.; Mazur, P. *Non-equilibrium Thermodynamics*; Dover Publications: New York, 1984.
(19) Brunet, E.; Ajdari, A. *Phys. Rev. E* **2004**, *69*, 16306.
(20) Lyklema, J.; Rovillard, S.; Coninck, J. D. *Langmuir* **1998**, *14*, 5659.
(21) Spohr, E. *Electrochim. Acta* **2003**, *49*, 23.
(22) Qiao, R.; Aluru, N. R. *Phys. Rev. Lett.* **2004**, *92*, 198301.
(23) Joseph, S.; Aluru, N. R. *Langmuir* **2006**, *22*, 9041.

(24) Kim, D.; Darve, E. *Phys. Rev. E* **2006**, *73*, 051203.
(25) Thompson, A. P. *J. Chem. Phys.* **2003**, *119*, 7503.
(26) Iler, R. K. *The Chemistry of Silica*; Wiley: New York, 1979.
(27) Dong, Y.; Pappu, S. V.; Xu, Z. *Anal. Chem.* **1998**, *70*, 4730.
(28) Shaw, A. M.; Hannon, T. E.; Li, F.; Zare, R. N. *J. Chem. Phys. B* **2003**, *107*, 7070.
(29) Fisk, J. D.; Batten, R.; Jones, G.; O'Reilly, J. P.; Shaw, A. M. *J. Chem. Phys. B* **2005**, *109*, 14475.
(30) Bolt, G. H. *J. Phys. Chem.* **1967**, *61*, 1166.
(31) Schindler, P. W.; Fürst, B.; Dick, R.; Wolf, P. U. *J. Colloid Interface Sci.* **1976**, *55*, 469.
(32) Behrens, S. H.; Grier, D. G. *J. Chem. Phys.* **2001**, *115*, 6716.
(33) Ong, O.; Zhao, X.; Eisenthal, K. B. *Chem. Phys. Lett.* **1992**, *191*, 327.
(34) van der Heyden, F. H. J.; Stein, D.; Dekker, C. *Phys. Rev. Lett.* **2005**, *95*, 116104.
(35) Tadros, T. F.; Lyklema, J. *J. Electroanal. Chem.* **1968**, *17*, 267.
(36) Karlsson, M.; Craven, C.; Dove, P. M.; Casey, W. H. *Aquat. Geochem.* **2001**, *7*, 13.
(37) Besteman, K.; Zevenbergen, M. A. G.; Lemay, S. G. *Phys. Rev. E* **2005**, *72*, 061501.
(38) Cruz-Chu, E. R.; Aksimentiev, A.; Schulten, K. *J. Phys. Chem. B* **2006**, *110*, 21497.
(39) Van Beest, B. W. H.; Kramer, G. J.; van Santen, R. A. *Phys. Rev. Lett.* **1990**, *64*, 1955.
(40) Lopes, P. E. M.; Murashov, V.; Tazi, M.; Demchuk, E.; MacKerell, A. D., Jr. *J. Phys. Chem. B* **2006**, *110*, 2782.
(41) Nangla, S.; Washton, N. M.; Mueller, K. T.; Kubicki, J. D.; Garrison, B. J. *J. Phys. Chem. C* **2007**, *111*, 5169.
(42) (a) Jorgensen, W. J.; Maxwell, D. S.; Tirado-Rives, J. *J. Am. Chem. Soc.* **1996**, *118*, 11225. (b) Jorgensen, W. J. Private communication, 2003.
(43) Travis, K. P.; Todd, B. D.; Evans, D. J. *Phys. A* **1997**, *240*, 315.
(44) Travis, K. P.; Gubbins, K. E. *J. Chem. Phys.* **2000**, *112*, 1984.
(45) Plimpton, S. *J. Comp. Phys.* **117**, *1*, 01995.
(46) Jorgensen, W. L.; Chandrasekhar, J.; Madura, L. T.; Impey, R. W.; Klein, M. L. *J. Chem. Phys.* **1983**, *79*, 926.
(47) Hoover, W. G. *Phys. Rev. A* **1985**, *31*, 1695.
(48) Yeah, I-C.; Hummer, G. *J. Am. Chem. Soc.* **2002**, *124*, 23.
(49) Koneshan, S.; Rasaiah, J. C.; Lynden-Bell, R. M.; Lee, S. H. *J. Phys. Chem. B* **1998**, *102*, 4193.
(50) Chandra, A.; Bagchi, B. *J. Chem. Phys.* **2000**, *113*, 3226.
(51) Berendsen, H. J. C.; Grigera, J. R.; Straatsma, T. P. *J. Phys. Chem.* **1987**, *91*, 6269.
(52) Guo, G.; Zhang, Y.; Zhao, Y. *Phys. Rev. E* **2003**, *67*, 43101.

JP711510K